The Energy Calibration of USA

Pablo Saz Parkinson

15 April 2001

Abstract

The following document is a report on the efforts to date in performing the energy calibration of USA. I used TVAC data from 1996, 1997 and 1998, as well as data in orbit of the iron calibration source and observations of the Crab nebula.

1 Introduction

The energy calibration of USA was carried out in several stages. Data was used from test runs performed on the ground over the course of several years using a known X-ray source. Some calibration data was taken in 1996, before the Detector Interface Board (DIB) was in place. This produced the highest resolution possible (128 channels). The observations on the ground were taken at different voltages, so I made sure the ones used were at the same nominal high voltage as in orbit, that is at 2776.5 V. Subsequent ground data was taken, with the DIB in place, in August, September and October of 1997 and in June of 1998. All this ground data was used to derive an initial calibration which was then verified with data taken in orbit. The calibration in orbit was done using several observations of blank skies in which the $^{55}_{26}$Fe source was placed in the field of view. Calibration in orbit introduced the added complication of subtracting the background (diffuse X-ray and other). In addition, the intensity of the X-ray source became an issue; the source had, by now, decayed to a rate of about 50-60 counts per second, compared to an initial rate of several thousand counts per second when the source was initially purchased (several years prior to the launch of USA). This meant that in many calibration observations taken in "high

background" parts of the orbit, the iron source was actually undetectable. Finally, we used observations of the Crab nebula, which has a fairly well determined energy spectrum, to determine the adequacy of our computed calibration.

2 On-ground calibration

2.1 Calibration source

The source used for the ground calibration was an iron ($^{55}_{26}$Fe) source. The iron source has a half-life of 2.73 years and through electron capture decays to $^{55}_{25}$Mn* (equation 1). The excited manganese atom then relaxes to the ground state by filling the vacancy in the inner orbit with an outer electron and producing an X-ray photon. It is these X-ray photons that we use as our calibration signal.

$$^{55}_{26}Fe + e^- \rightarrow ^{55}_{25} Mn^* + \nu \rightarrow ^{55}_{25} Mn + \gamma \quad (1)$$

Table 1 summarises the three main transitions with their relative intensities (taken from [2]).

2.2 Escape peak

If the energy of the incoming X-rays is greater than the binding energy of the K shell of the detector gas, it can produce characteristic X-rays from the gas which are detected as a lower energy "escape peak". For argon, the binding energy of the K shell is 3.203 KeV, so the ejected K shell electron will have an energy of roughly 2.69 KeV when the incoming photon is 5.9 KeV. When the L shell electron in argon drops down to fill the K shell, a 2.956 KeV photon is produced (for Argon $K = 3.203$ KeV, $L_{II} = 0.247$ KeV, see [2]). If this photon "escapes" the gas, the energy left from the original X-ray will be decreased by this amount. To summarise, we expect our $^{55}_{26}$Fe calibration source to produce four peaks: two main peaks at roughly 5.9 KeV and 6.5 KeV along with their respective (and much smaller) escape peaks at 2.94 KeV and 3.53 KeV. Figures 1 and 2 show these individual peaks from ground data taken in 1996 when we had 128 "raw" channels of resolution. In later data, with the DIB in place, our effective resolution is greatly reduced

and we therefore resort to fitting the data with only two gaussians, instead of four.

Name	Transition	Energy (KeV)	Relative Intensity
K_{α_1}	$2^2P_{3/2} \rightarrow 1^2S_{1/2}$ $(n = 2 \rightarrow n = 1)$	5.898	100
K_{α_2}	$2^2P_{1/2} \rightarrow 1^2S_{1/2}$ $(n = 2 \rightarrow n = 1)$	5.887	51
K_{β_1}	$3^2P \rightarrow 1^2S_{1/2}$ $(n = 3 \rightarrow n = 1)$	6.490	16

Table 1: Radioactive transitions of the $^{55}_{25}$Mn atom

2.3 1996 Ground Data

Figure 1 shows a fit to some 1996 ground data. The two main gaussians, in red and blue, represent iron lines at 5.9 KeV (which is actually a blend of two lines of very similar energies) and 6.5 KeV (see table 1), as observed in layer 1 of the detector . The mean, 43.66 and 48.14 respectively, is expressed in channels out of 128. Figure 2 shows the best fit to the layer 2 spectrum. Once again, we see the main peak at 5.9 KeV, and a smaller one at 6.5 KeV, along with the corresponding escape peaks.

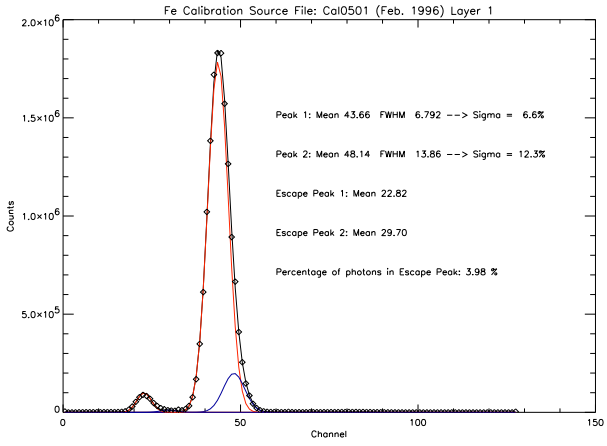

Figure 1: Fe calibration source (2 lines): Layer 1

Given the limited resolution of our in-orbit data, it becomes hard to fit the calibration data with four gaussians. We therefore decided to fit only one main peak and its escape peak. Figures 3 and 4 show such a fit to the same data as that shown in figures 1 and 2. Using the relative intensities of the lines (from table 1) we arrive at a mean energy of 5.95 KeV for the blend of the three lines.

As can be seen from the figures, the result of considering the spectrum as one gaussian instead of two is to effectively shift the line up to a slightly higher energy (5.95 vs 5.9) and increase the standard deviation of the gaussian by a small amount.

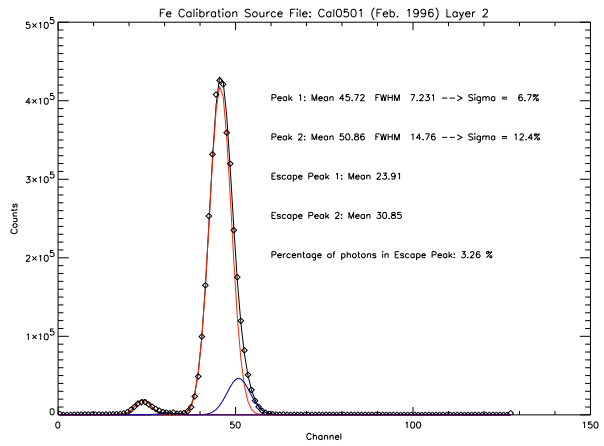

Figure 2: Fe calibration source (2 lines): Layer 2

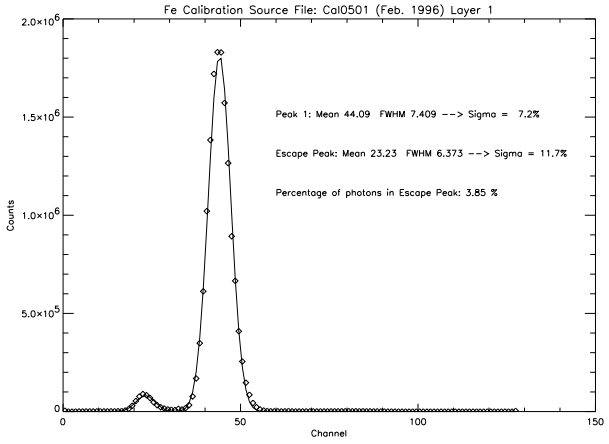

Figure 3: Fe calibration source: Layer 1

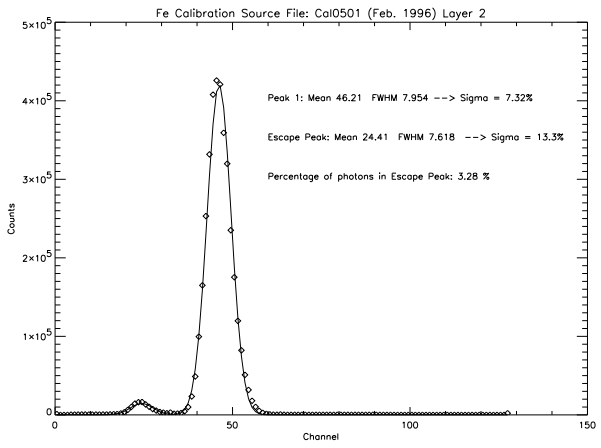

Figure 4: Fe calibration source: Layer 2

2.4 1997 Ground Data

Figures 5 and 6 show a fit to some 1997 ground data (layers 1 and 2 respectively). This data was taken with the DIB already in place, and therefore the number of channels is now greatly reduced (16 vs 128). One key difference with the 1996 ground data is the location of the iron peak. In figure 5 we find the mean in channel 6.40 (figure 6 shows layer 2 peaking in channel 6.07). By comparison the 1996 observations show the layer 1 peak (see figure 3) in channel 44.09 (or channel 5.51 in a 16 channel scale), and the layer 2 peak (see figure 4) in channel 46.21 (5.78 in a 16 channel scale). Even more confusingly, some 1997 data (see figure 7) shows the layer 1 peak in channel 5.47. This issue needs to be resolved.

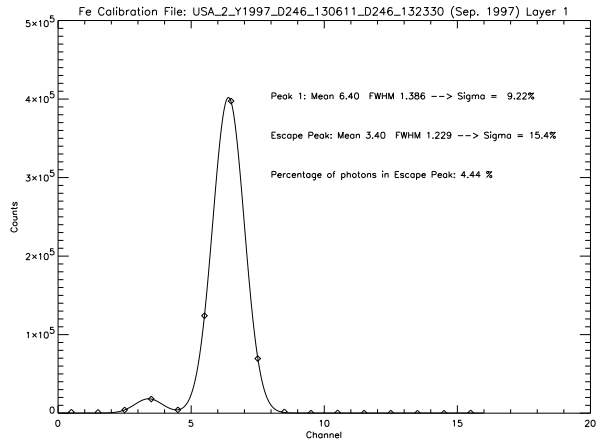

Figure 5: Fe Source 1997 TVAC : Layer 1

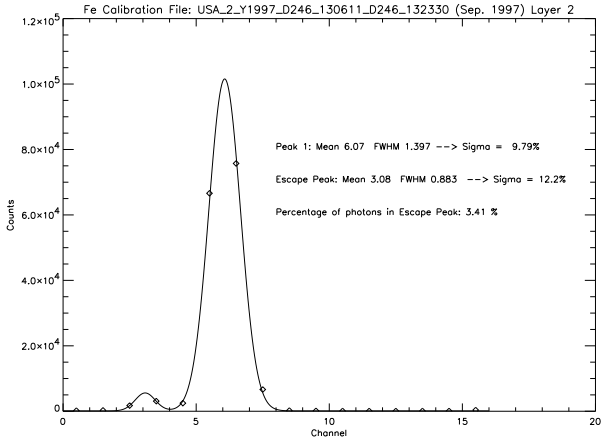

Figure 6: Fe Source 1997 TVAC : Layer 2

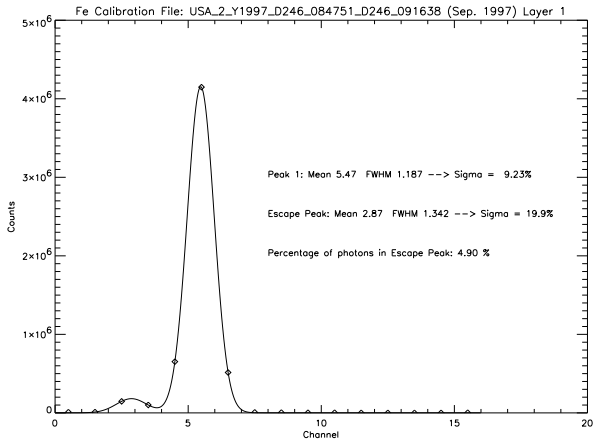

Figure 7: Fe Source 1997 TVAC : Layer 1

2.5 1998 Ground Data

We also looked at some TVAC data taken in June of 1998. As with the 1997 data, given the poor resolution (16 channels), we decided to fit the energy spectrum of the calibration source with two gaussians: one for the main peak at 5.95 KeV and one for the escape peak.

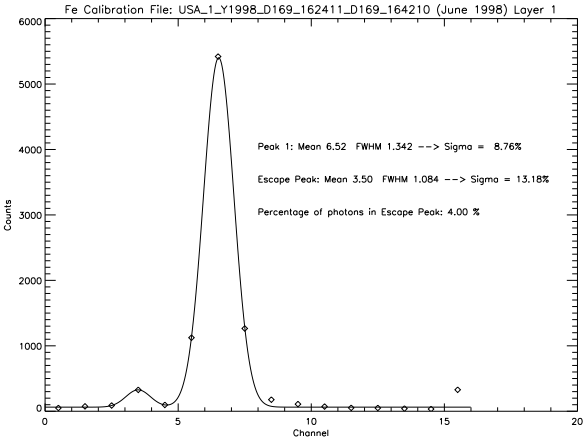

Figure 8: Fe Source 1998 TVAC : Layer 1

Figures 8 and 9 show the fits to the layer 1 and layer 2 spectra respectively. Once again, the key parameter to notice is the channel where the energy

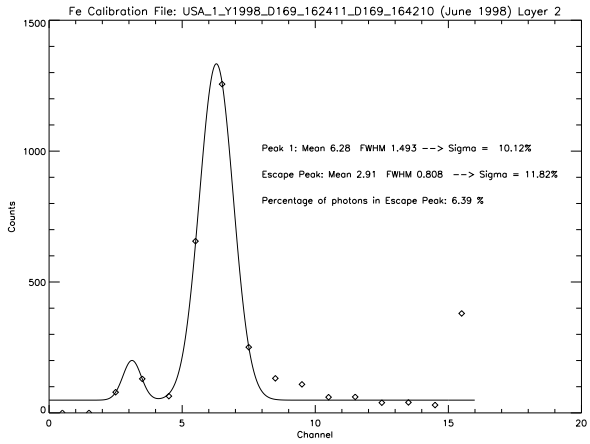

Figure 9: Fe Source 1998 TVAC : Layer 2

spectrum peaks. Figures 8 and 9 show the layer 1 spectrum peaking in channel 6.52, and the layer 2 spectrum peaks in channel 6.28. This conflicts with the results obtained from the 1996 data and some of the 1997 data, but agrees with some of the 1997 ground data. It appears that the iron line in layer 1 of our detector varies its position from around channel 5.5 to 6.5.

3 In-orbit calibration

The following figures show two typical calibration observations. Figure 10 represents an observation taken on the ascending side of the orbit, while figure 11 was taken on the descending part of the orbit. The observations normally consist of roughly 80 seconds of blank sky, followed by about 100 seconds of the calibration ($^{55}_{26}$Fe) source. For each observation I obtained a rough estimate of the background in each layer, subtracted this background and then fit a gaussian to the resulting spectrum. As can be seen from these two observations, the peak in layer 1 falls about one channel higher in the ascending observation than in the descending one - a 20% difference in gain. Layer 2 does not show this dramatic difference.

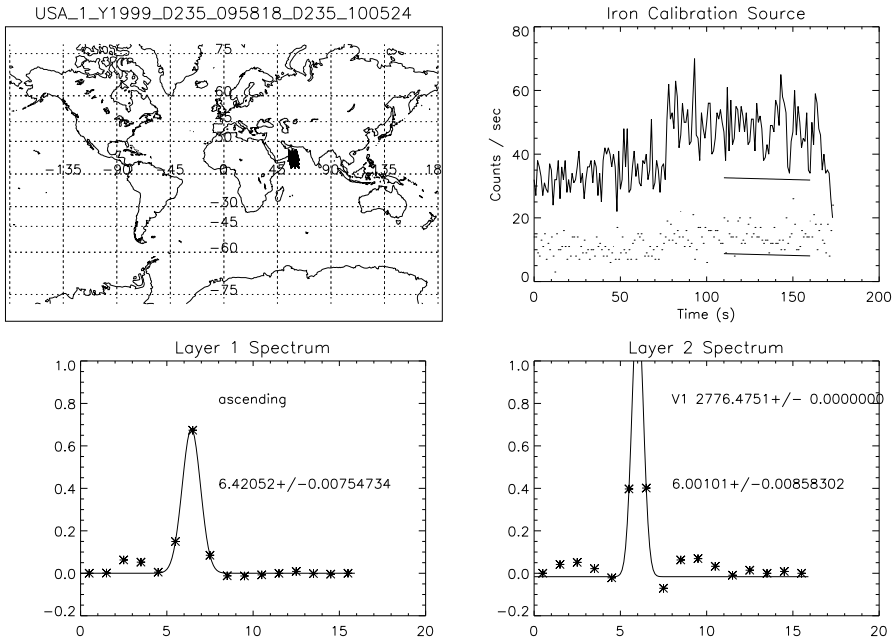

Figure 10: Typical Ascending Observation: Top Left: Location of ARGOS during the observation, Top Right: Layer 1 (solid line) and Layer 2 (dotted line) Lightcurve, Bottom Left: Layer 1 Spectrum and fit, Bottom Right: Layer 2 Spectrum and fit. Numbers on bottom plots represent mean of gaussian fit.

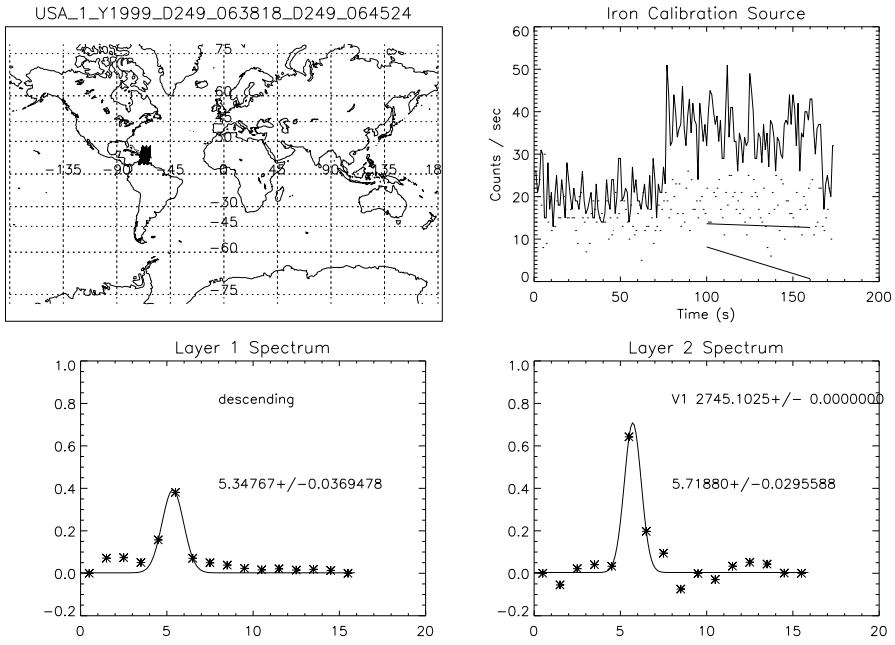

Figure 11: Typical Descending Observation: Top Left: Location of ARGOS during the observation, Top Right: Layer 1 (solid line) and Layer 2 (dotted line) Lightcurve, Bottom Left: Layer 1 Spectrum and fit, Bottom Right: Layer 2 Spectrum and fit. Numbers on bottom plots represent mean of gaussian fit.

Figure 12 shows the values of the gaussian mean obtained from fitting the layer 1 spectra as described in the previous section to about 75 individual calibration observations. Each point represents one of these calibration observations. While there are large gaps in the coverage, the observations span roughly 400 days. Red points represent ascending observations, while blue points represent descending observations. These form two distinct populations. Figure 13 shows the same information for layer 2, though it is apparent that the effect is much less pronounced, if it is present at all.

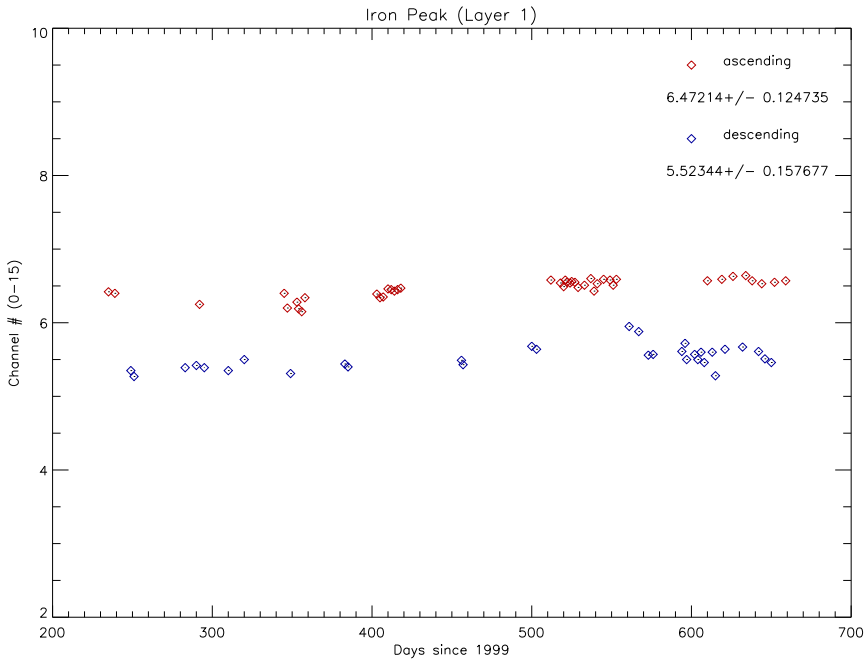

Figure 12: Fe Calibration Main Peak: Layer 1. Every point represents a calibration source observation. Red dots were taken in the ascending-node orbits and blue dots were taken in the descending-node orbits

3.1 Copper Fluorescence

In looking at some blank sky observations, we noticed a peak in the energy spectrum which we interpreted as a copper fluorescence line (the USA

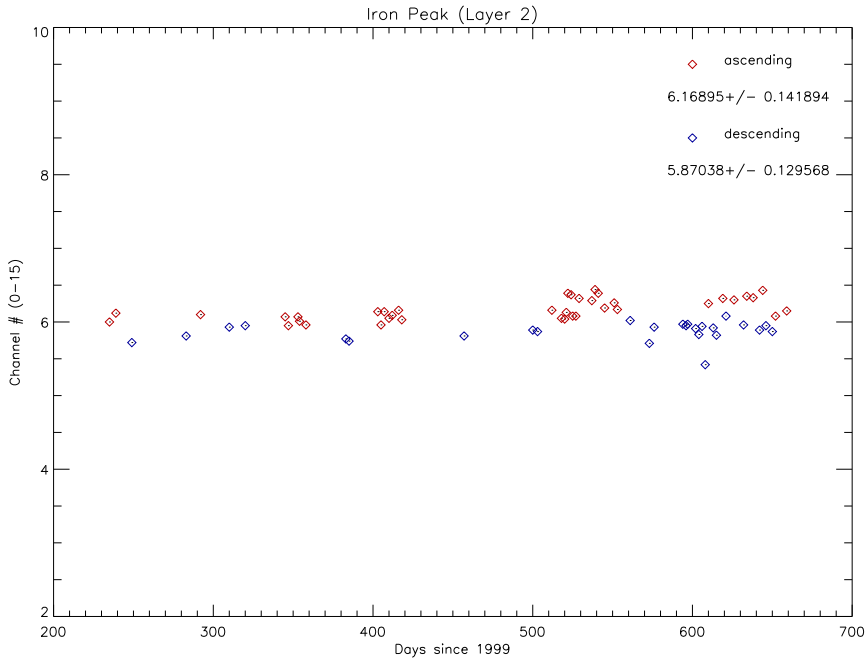

Figure 13: Fe Calibration Main Peak: Layer 2. Every point represents a calibration source observation. Red dots were taken in the ascending-node orbits and blue dots were taken in the descending-node orbits

collimator is made of copper). Figures 14 through 17 show a series of blank sky segments (each 100 seconds long) which have been averaged and then fit with an exponential plus a gaussian. We then attempted to use this line, which corresponds to 8.03 KeV (see [2]), to improve our energy calibration. To verify that the copper fluorescence line was at least in part due to background particles colliding with the detector. In figure 18 we plot the ratio of counts in channels 5-7 (which is where the peak roughly lies) to total counts versus the difference between counts in both layers of channel 15. This last quantity is a measure of the intensity of soft electrons. The plot shows that the intensity of this copper line was indeed correlated with the number of soft electrons, though the correlation is not particularly strong.

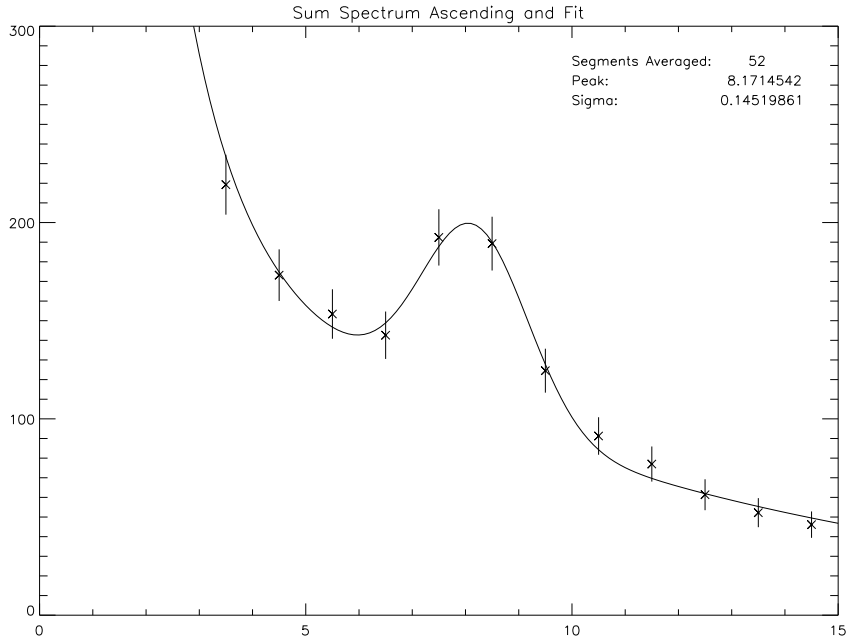

Figure 14: Cu Fluorescence Peak (ascending): Layer 1

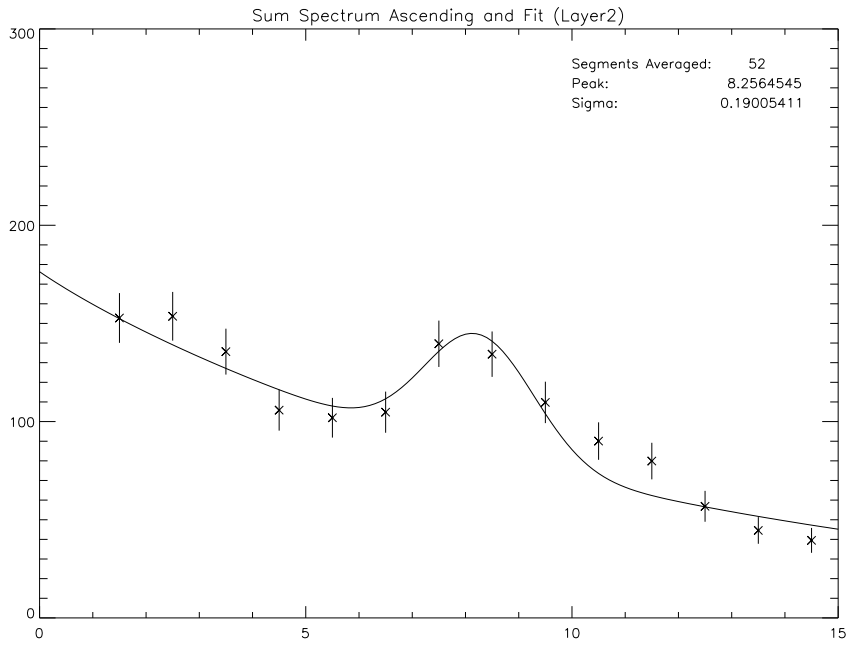

Figure 15: Cu Fluorescence Peak (ascending): Layer 2

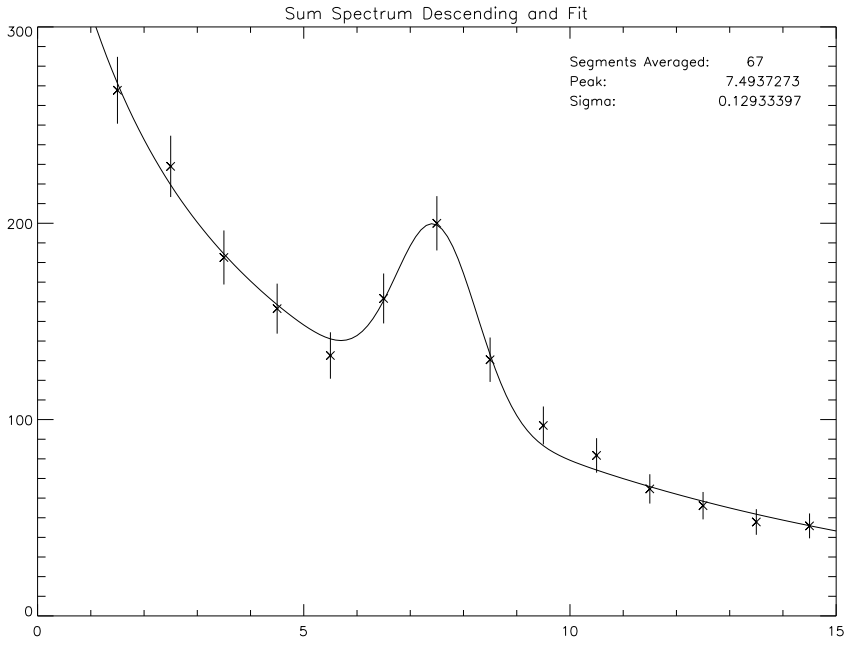

Figure 16: Cu Fluorescence Peak (descending): Layer 1

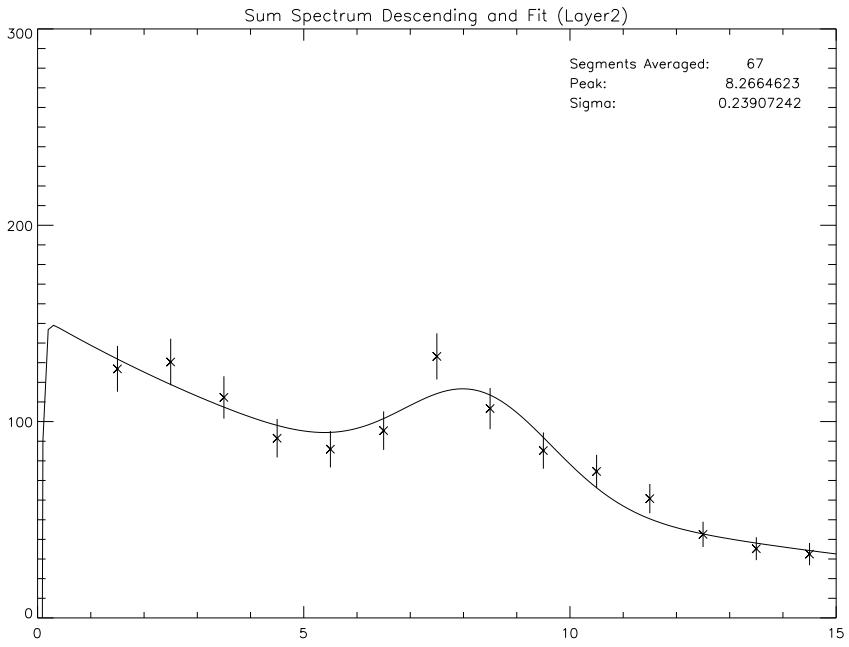

Figure 17: Cu Fluorescence Peak (descending): Layer 2

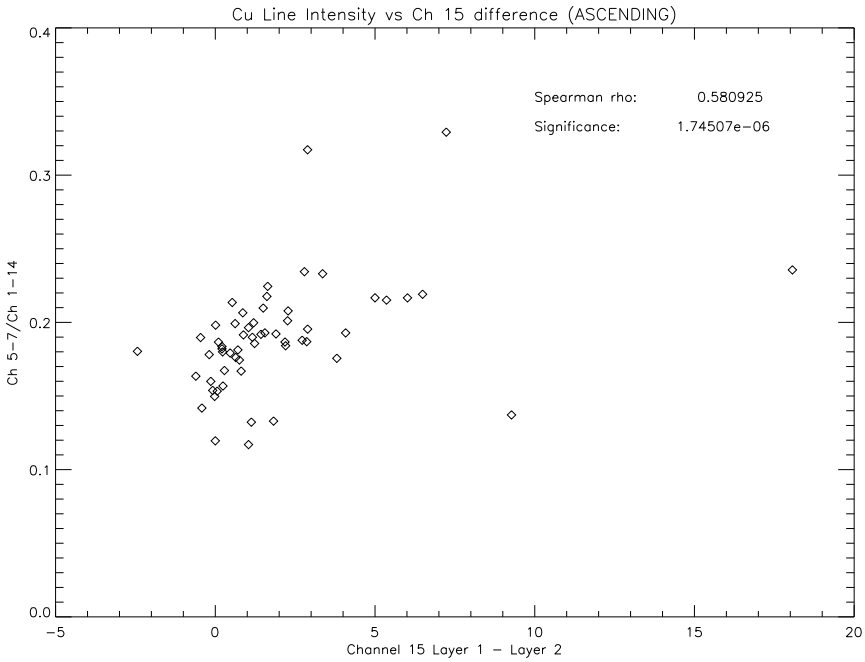

Figure 18: Cu Fluorescence correlation with soft electrons

3.2 Orbital dependence of the gain

Given the clear difference in gain detected between the ascending and descending observations, and given that USA is always in the dark in descending orbits and in the sun in ascending ones, it would seem natural to interpret this effect as being temperature related. In the absence of convection, it is plausible that a temperature gradient could be maintained between the two different layers of the chamber (which are nevertheless connected, and therefore would quickly reach a thermal equilibrium on the ground where convection is present). The question we ask ourselves, therefore, is how large a temperature gradient do we need to cause the observed 20% effect in gain?

We begin by writing down the first order differential equation which describes the dependence of the gain on the voltage and the density. A change in voltage implies a change in electric field strength (which is proportional to V) and therefore an increase in gas amplification. Conversely, an increase in pressure (or decrease in density) increases the mean free path, and, once again, increases the amplification in the gas. In the proportional region of the gas (where USA operates), we can write:

$$\frac{dG}{dV^*} = \alpha G \tag{2}$$

where we have defined:

$$V^* = \frac{V}{\rho} \tag{3}$$

and therefore:

$$dV^* = -\frac{V}{\rho^2}\, d\rho \tag{4}$$

Separating variables in equation 2 and integrating, we obtain:

$$\frac{dG}{G} = \alpha\, dV^* \tag{5}$$

$$\int \frac{dG}{G} = \ln G = \alpha V^* + C = \int \alpha\, dV^* \tag{6}$$

We use the fact that for P-10 (90% Ar, 10% CH_4) in the proportional region, a change in voltage of 100 V has the effect of doubling the gain:

$$2Ce^{\frac{\alpha V_0}{\rho}} = Ce^{\frac{\alpha (V_0+100)}{\rho}} \tag{7}$$

from which we deduce that:

$$\alpha = \rho \frac{\ln 2}{100} \tag{8}$$

Substituting equations 8 and 4 into 5 we obtain the following:

$$\frac{dG}{G} = -V \frac{\ln 2}{100} \frac{d\rho}{\rho} \tag{9}$$

From the ideal gas law, we have:

$$PV = NkT \tag{10}$$

$$\rho = \frac{N}{V} \tag{11}$$

$$T = \frac{P}{\rho k} \tag{12}$$

$$\frac{dT}{T} = -\frac{d\rho}{\rho} \tag{13}$$

Finally, substituting this into equation 9, we get:

$$\frac{dG}{G} = V \frac{\ln 2}{100} \frac{dT}{T} \tag{14}$$

$$\Delta T \approx \frac{100T}{V \ln 2} \frac{\Delta G}{G} \tag{15}$$

where $\frac{\Delta G}{G}$ is the observed change in gain of around 20% between the ascending and descending node observations, V is the chamber voltage, which is roughly held constant at around $2775V$ and T is the temperature of the chamber, which is around $285K$. Entering all these numbers, we arrive at:

$$\Delta T \approx \frac{(100)(285K)}{\ln 2(2775V)}(0.20) \approx 3K \tag{16}$$

3.3 Observed Temperature Gradient

The following plots show the temperatures of the back plate (UD1TBP) and that of the thermocouple located inside the chamber (USAST4) plotted together, for the times which span the calibration observations shown in figures 10 and 11. The vertical line shows roughly where the calibration observation would fall. As can be noted, in the first observation we see a temperature gradient of around 2.5-3K, whereas in the second case there is essentially no temperature gradient. It is interesting to note that throughout the several orbits displayed in figure 10 there is a clear temperature gradient whenever USA is on the ascending side, whereas there is virtually no temperature gradient when USA is descending (at least in the part of the orbit where USA would be observing, i.e. between the belts). The phase lag between the two temperature curves is consistent with the fact that the "back" takes longer to heat up, and therefore to cool down than the "front"

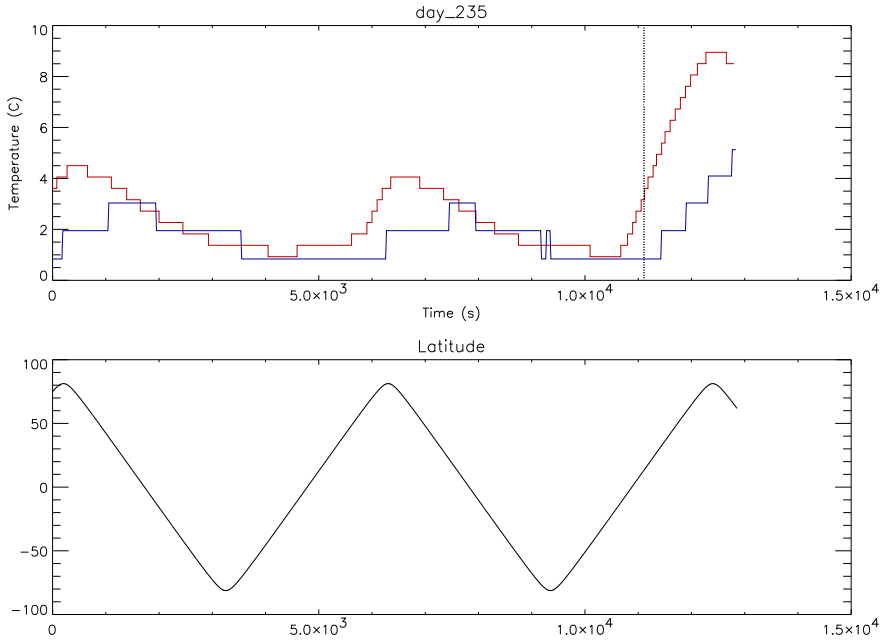

Figure 19: Day 235 (Ascending)

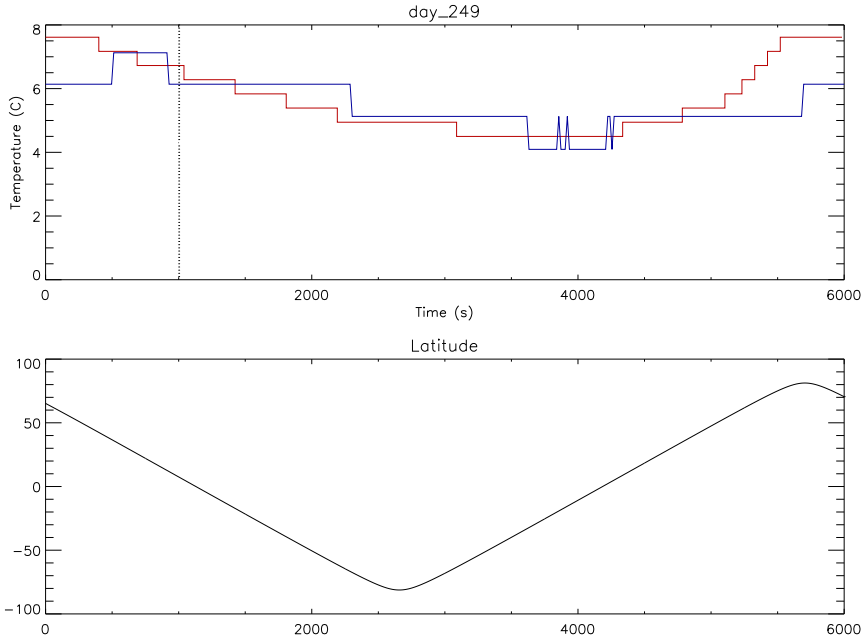

Figure 20: Day 249 (Descending)

4 USA response matrices

The response matrix is a fits file which contains the arrays describing the characteristic response of USA to incoming X-rays. The response matrices are required by XSPEC, in combination with the observed source spectrum and a model spectrum, to perform spectral fits. As its name implies, it is a matrix, and it has the form R(I,E), essentially giving the probability that an incoming photon of energy E will be detected in channel I (for more details see [1]). In order to create these matrices, two main aspects of the instrument must be considered: the gain (which will determine the energy boundaries) and the detector efficiency. Using our calibration sources, we first created a raw (128 channels) energy to channel conversion. We then rebinned this into the different USA modes. Table 2 describes the total of seven response matrices that were finally created. Due to the unforseen problem of temperature dependent gain variations, a different set of seven response matrices was created for ascending and descending node observations, bringing the total number of response matrices to 14.

Filename	Modes	Layers	Number of channels
usa_d1_l1_m1.rsp	1 and 2	1	16
usa_d1_l2_m1.rsp	1 and 2	2	16
usa_d1_l1_m3.rsp	3 and 4	1	8
usa_d1_l2_m3.rsp	3 and 4	2	8
usa_d1_m1.rsp	1 and 2	1 and 2	16
usa_d1_m3.rsp	3 and 4	1 and 2	8
usa_d1_m5.rsp	5	1 and 2	47

Table 2: USA response matrices

For now, the most up-to-date response matrices are available at the anonymous ftp site:

ftp://ftp.slac.stanford.edu/groups/ek/pablos/response_matrices/

There are two subdirectories (/ascending and /descending) which contain the appropriate set of matrices for ascending and descending node observations.

4.1 USA modes

USA has five possible modes of observing: four "timing" modes (1 through 4) and a "spectral" mode (5). Modes 1 and 2 have 16 channels which are binned linearly and therefore every channel corresponds to 8 "raw" channels. Modes 3 and 4 have only 8 channels, also binned linearly, so each of these channels will correspond to 16 of the original 128 "raw" channels. Mode 5 is a little more complicated as it is binned more heavily in the low energy regime. It has 47 channels. The first 30 channels correspond to the first 60 raw channels (i.e. 2 "raw channels" per channel) and the last 17 channels correspond to the last 68 (i.e. 4 "raw channels" per channel).

4.2 Energy to channel conversion

A key step in building the response matrices is determining the gain of the instrument, which in turn determines the energy to channel conversion. Figure 21 shows our linear fits to the observed in-orbit data. The key data points represent the iron line, its escape peak, and the copper fluorescence peak. We show the fits for ascending and descending observations, both for layers 1 and 2 separately. For our layer 2 fits we did not include the copper fluorescence line, given the poor quality of our fit to such a line (see figures 15 and 17). For our layer 1 fits we used the mean value in our fit (figures 14 and 16) to represent the 8.03 KeV copper line. The mean iron line was obtained from the in-orbit blank sky observations (figures 12 and 13). We chose a linear fit due to the scarcity of data points, but also due to the fact that USA is, after all, a "proportional" chamber, and therefore the deviations from linearity should be small.

4.3 USA effective area

The gas used in USA is P10, that is 90% argon and 10% methane (CH_4). The efficiencies of the gas were computed by M. Kowalski at NRL and independently by G. Godfrey at SLAC. The nominal temperature and pressure at which these were computed were 22 degrees C and 15.8 psi. The densities were taken from [5]. Mylar, Nichrome IV, and gas densities were calculated by M. Kowalski and verified by comparison to a data table obtained from D.J. Yentis. Table 3 shows the different window and gas thicknesses traversed by an incoming X-ray, along with the densities of the corresponding materials..

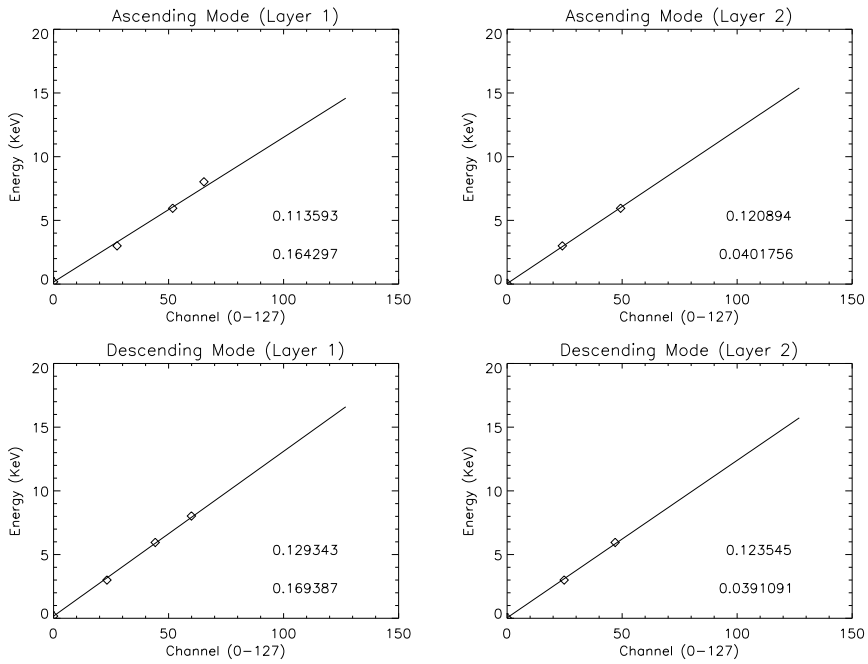

Figure 21: Energy to Channel Fit: Top Left: Ascending Node (Layer 1), Top Right: Ascending Node (Layer 2), Bottom Left: Descending Node (Layer 1), Bottom Right: Descending Node (Layer 2). Top number represents the slope of the line, bottom number represents the offset.

The thickness of each of the two layers of gas is 3.094 cm, bringing the total thickness for both layers to 6.1880 cm.

Chemical formula of Material	Thickness	Density (g/cm^3)
Al	0.0800 microns	2.694 (Bulk)
$C_{10}H_8O_4$	1.8300 microns	1.397
$C_{10}H_8O_4$	5.0000 microns	1.397
Ni_8Cr_2	0.0028 microns	8.5
Ar_9CH_4	6.1880 cm	1.63E-3

Table 3: USA window and gas thicknesses and densities (both layers)

The effective area is obtained by multiplying the efficiency by the geometrical area and the collimator response. The geometrical area used for one detector was 1286 cm^2 and the collimator being used has a flat-top efficiency of 0.88.

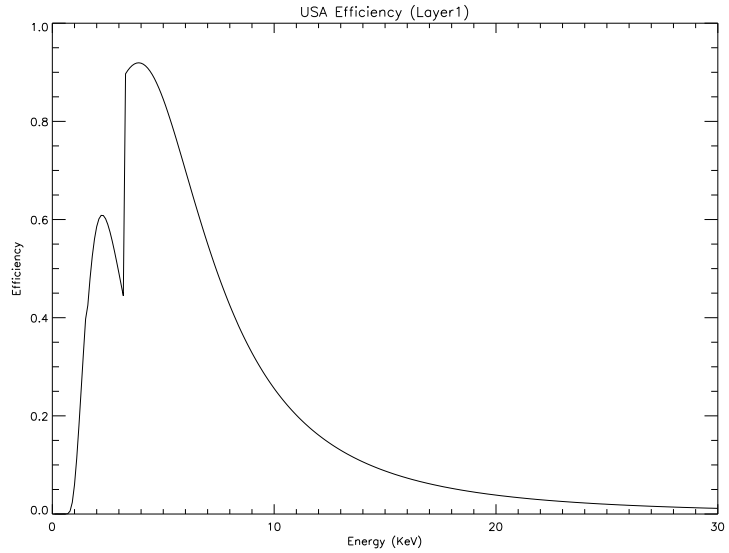

Figure 22: USA efficiency: Layer 1

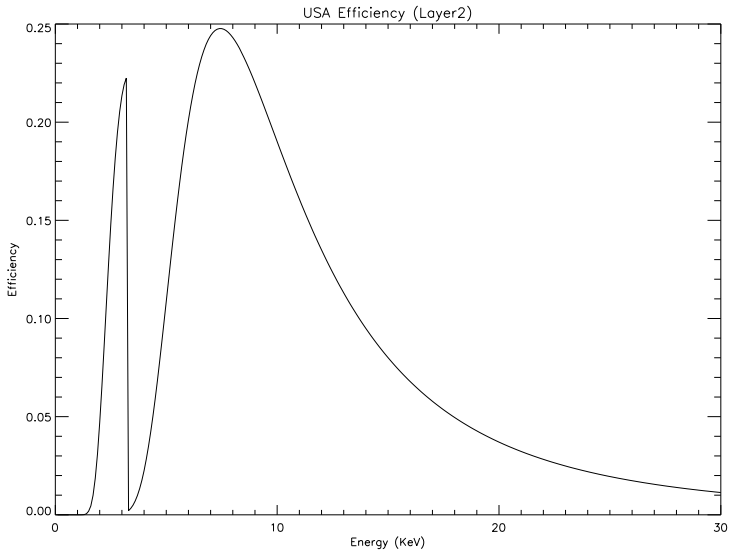

Figure 23: USA efficiency: Layer 2

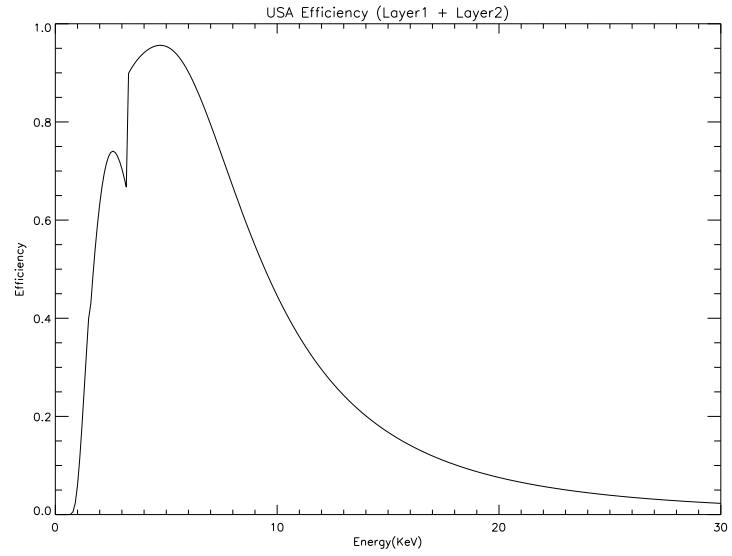

Figure 24: USA efficiency: Both layers

4.4 Crab Energy Spectrum

The Crab Nebula represents a sort of standard X-ray source which has been used for calibrating most X-ray telescopes for the last 30 years. The X-ray emission from the diffuse region of the Crab appears to be constant, to within 10% (see [3] for more details). Toor & Seward ([4]) used 28 different spectra obtained from rocket and balloon experiments to derive an absolute calibration for the Crab to within 10%. The spectrum they obtained between 2 and 60 KeV is:

$$I(E) = 9.7 \pm 1.0 E^{-2.10 \pm 0.03} ph/cm^2/sec/KeV \tag{17}$$

Figure 25 shows a fit to the Crab energy spectrum (this particular observation was in the ascending node). We used an absorbed power law as the model, and froze the power law index at the canonical 2.1 value. As can be seen from the residuals, the fit is roughly within 10% for energies above 2.5 KeV, but is not so good for energies below this. There is a sinusoidal shape to the residuals which suggests that the energy boundaries in our current calibration are not quite right.

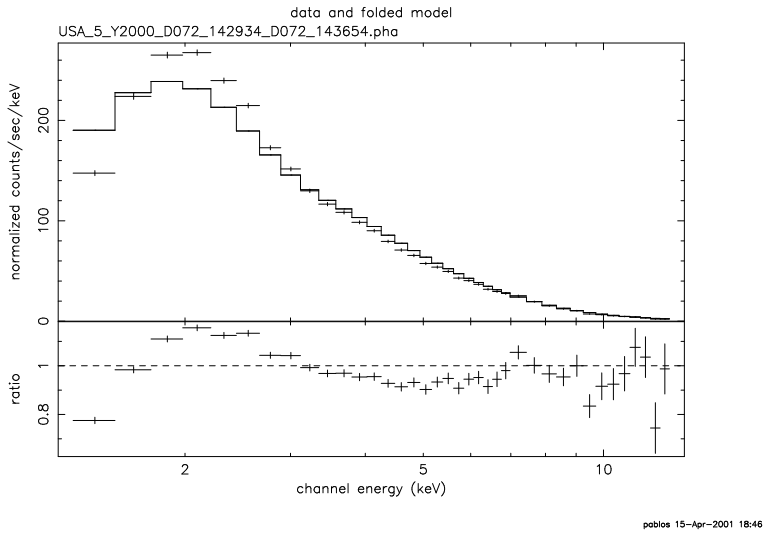

Figure 25: Crab Energy Spectrum USA_5_Y2000_D072_142934_D072_143654. Observation was in the ascending node. Fit to an absorbed powerlaw with index of 2.1.

5 Conclusions

An energy calibration of USA was carried out with 1996 ground data, which provided the highest resolution (128 channels). This calibration was then checked with calibration data taken in orbit and was found to be in significant disagreement. Specifically, we found a different energy calibration was required for ascending and descending node observations. The 1996 ground calibration appears to be consistent with the descending node in-orbit calibration. We further checked our energy calibration with 1997 and 1998 TVAC data. At times this data seemed to be consistent with the ascending node in-orbit calibration and other times consistent with the descending node calibration. The source of such discrepancies needs to be further investigated. The current USA response matrices were built using in-orbit data. We used the peak of the iron calibration source as well as the observed copper fluorescence peak to produce a linear fit for the gain in both ascending and descending node observations. Using these fits and the USA efficiencies, we built two sets of response matrices, one for each of the ascending and descending sides of the orbit. Finally, we used our response matrices in XSPEC to fit the Crab energy spectrum with a power law of index of 2.1, which gave us an idea of how our current energy calibration performs on a well determined spectrum.

References

[1] K. Arnaud and B. Dorman. *XSPEC. An X-Ray Spectral Fitting Package. User's guide Version 11.* 2000.

[2] J.M. Hollander C.M. Lederer and I. Perlman. *Table of Isotopes. Sixth Edition.* John Wiley & Sons, 1967.

[3] N.J. Westergaard H.U. Noergaard-Nielsen, C. Budtz-Joergensen and H.W. Schnopper. Excalibur - absolute calibration of the x-ray spectrum of the crab nebula. *A&A*, 285:705–709, May 1994.

[4] A. Toor and F.D. Seward. The crab nebula as a calibration source for x-ray astronomy. *AJ*, 79:995–999, October 1974.

[5] Vigele. *Atomic Data Tables, vol. 5.* 1973.